Unsteady Supersonic Computations of Arbitrary Wing-Body Configurations Including External Stores

P. C. Chen*
Zona Technology, Inc., Mesa, Arizona
and
D. D. Liu†
Arizona State University, Tempe, Arizona

A general harmonic gradient method has been developed for computations of unsteady supersonic flow handling given wing-body combinations, including arbitrary external store arrangements. The harmonic gradient model is adopted so that the total panel number is least affected by the given Mach number and reduced frequencies. To assess the accuracy and effectiveness of the present method, comparison with available data is given including the National Aerospace Laboratory's measurements for underwing store and wing-with-tip missile cases. The accurate prediction and ease of application of the present method suggests that it is fully developed for supersonic aeroelastic applications to realistic aircraft configurations.

Nomenclature

A = panel area
$C_{p(n)}$ = pressure coefficient
h_B = (h_B, h_B', h_B'') body structural mode, slope, and curvature
h_w = wing structural mode parallel to the outward normal vector
k = KM/β, K is the reduced frequency
M = freestream Mach number
n = (n_x, n_y, n_z) unit outward normal vector of each panel
u = (u_0, v_0, w_0) steady mean velocity on the body
V_B = total velocity on the body
V_w = total velocity on the wing surface
x_0, y_0, z_0 = location of the control point
β = $(M^2-1)^{1/2}$
ζ = z_0-z
η = y_0-y
λ = unknown doublet strength
ξ = x_0-x
σ = unknown source strength
τ = body thickness ratio

Subscripts

$(\cdot)_i$ = $(\cdot)$ of the ith panel
$(\cdot)_j$ = $(\cdot)$ of the jth panel

Superscripts

$(\cdot)^{(I)}$ = $(\cdot)$ of the Ith structural mode
$(\cdot)^{(J)}$ = $(\cdot)$ of the Jth structure mode

Introduction

THE problem of the store-tip/missile-airframe interaction during the cruise or the maneuver phase of the supersonic fighter aircraft has been a major concern for design and analysis. It is known that this type of interaction will change the unsteady airload and, hence, alter the flutter characteristics of the wing/tail drastically. For example, problems such as underwing pylon/stores performing combined pitch-yaw oscillations and the tip missile/wing interference are among the critical factors to aircraft flutter. When an aircraft is in short-period, rigid-body motions, the effects of wing-fuselage interference on the damping-in-pitch derivative can be substantial. All such interfering cases considered warrant an accurate method in predictions of unsteady aerodynamics, stability derivatives, and flutter boundaries.

Although four decades of supersonic flight have passed, it appears that no satisfactory method exists in the prediction of supersonic unsteady airloads for such realistic wing-body configurations. Unsteady subsonic methods for computations of interference aerodynamics have been sufficiently developed in the past, notably the doublet lattice method.[1] By contrast, development in its supersonic counterpart only remains in methods for treating wing-alone[2-9] or body-alone[10-12] configurations. A low-order panel method for wing-body combinations has been previously formulated by Morino et al.,[13] but it presents insufficient unsteady results for assessment of its applicability.

On the other hand, computational methods for wings with external stores have been in urgent demand in recent years. Although some progress has been made in this area,[14,15] the methods employed are not yet fully developed to handle supersonic aeroelastic applications for arbitrary wing-body configurations including external stores.

In this paper, recent development of a supersonic panel method is presented for unsteady aerodynamic computations of arbitrary wing-body combinations with additional external-store systems. The present wing-body formulation is an outgrowth of the previous harmonic gradient method (HGM) for planar/nonplanar wing planforms.[9] Source panels are applied on the body surface, whereas doublet panels are used to model multiple lifting surfaces. In essence, the present approach could be considered as an unsteady generalization of Woodward's USSAERO method,[16] with the exception of the wing-thickness effect. The present method is completely general in the reduced frequency range, the body and wing planform geometries, and the structure mode inputs. The computer program is structured in such a way that the mode inputs and the unsteady aerodynamic outputs for the body part and the wing part can be independently accessed and maintained. In

Presented as Paper 88-2309 at the AIAA/ASME/ASCE/AHS 29th Structures, Structural Dynamics and Materials Conference, Williamsburg, VA, April 18-20, 1988; received May 9, 1988; revison received April 3, 1989.

*President. Member AIAA.
†Associate Professor. Member AIAA.

this way, the contributions due to wing-body interference can be conveniently assessed.

To validate the present method, various computed examples including wing-alone, body-alone, and different wing-body combinations in both steady and unsteady flows were selected for comparison with available data. For complex wing-body configurations, computed forces and moments for cases of a wing-with-tip missile and a wing with launcher/pylon/store in pitching oscillations were verified with those measured by the National Aerospace Laboratory (NLR).[17]

Approach

Kernel Evaluation and Paneling Scheme

First, the body surfaces are discretized into *NB* number of panels and each body panel is represented by a constant source distribution. This body-paneling scheme is considered as the generalization of the USSAERO method. The wing planforms are modeled by lifting surfaces, upon which the paneling scheme is set up according to the HGM arrangement,[9] as shown in Fig. 1.

Let the supersonic perturbed potential be represented by ϕ at the ith control point located either on the wing or the body. Thus, ϕ can be expressed as

$$\phi(x_0,y_0,z_0)=\sum_{j=1}^{NB}\phi_{Bj}\sigma_j+\sum_{j=1}^{NW}\phi_{wj}\lambda_j \tag{1}$$

where

$$\phi_{Bj}=\int_{\Delta\xi}\int_{\Delta\eta}e^{-ikM\xi}H(\xi,\eta,\zeta;\,k,M)\,d\eta\,d\xi \tag{2}$$

$$\phi_{Wj}=\int_{\Delta\eta}\int_{\Delta\xi}e^{-ikM\xi}\frac{\partial}{\partial n}H(\xi,\eta,\zeta;\,k,M)\,d\xi\,d\eta \tag{3}$$

ϕ_{Bj} and ϕ_{Wj} are the body potential and the wing potential, respectively, and

$$H(\xi,\eta,\zeta;\,ik,M)=\cos(kR)/R$$

where R denotes the hyperbolic distance between the control point and the field point, i.e., $R=(\xi^2-\eta^2-\zeta^2)^{1/2}$, and $\Delta\eta$ and $\Delta\xi$ define the boundaries of the jth panel (see Fig. 1).

The doublet kernel integral [Eq. (3)] is to be solved according to HGM. The source kernel integral is derived as follows:

An exact solution exists for the inner integral of Eq. (2); thus,

$$\phi_{Bj}=\int_{\Delta\xi}e^{-ikM\xi}\psi\,d\xi \tag{4}$$

where

$$\psi=J_0(kr)\sin^{-1}\left(\frac{\eta}{r}\right)+\sum_{n=1}^{\infty}\frac{(-1)^n}{n}J_{2n}(kr)\sin\left[2n\sin^{-1}\left(\frac{\eta}{r}\right)\right]$$

$$r=(\eta^2+\zeta^2)^{1/2}$$

and J_0, J_{2n} are the Bessel function of the first kind. Since ψ is a regular function bounded by the forwarded Mach cone, Eq. (4) can be solved numerically by means of a standard method such as Gaussian quadrature.

The velocity influence coefficients (VIC) are derived by differentiating Eq. (4) with respect to x_0, y_0, and z_0, respectively, i.e.,

$$\phi_{x_{Bj}}=\frac{\partial\phi_{Bj}}{\partial x_0}=-ikM\int_{\Delta\xi}e^{-ikM\xi}\psi\,d\xi+\int_{\Delta\xi}e^{-ikM\xi}\frac{\partial}{\partial x_0}(\psi)\,d\xi \tag{5}$$

$$\phi_{y_{Bj}}=\frac{\partial\phi_{Bj}}{\partial y_0}=\int_{\Delta\xi}e^{-ikM\xi}H\,d\xi \tag{6}$$

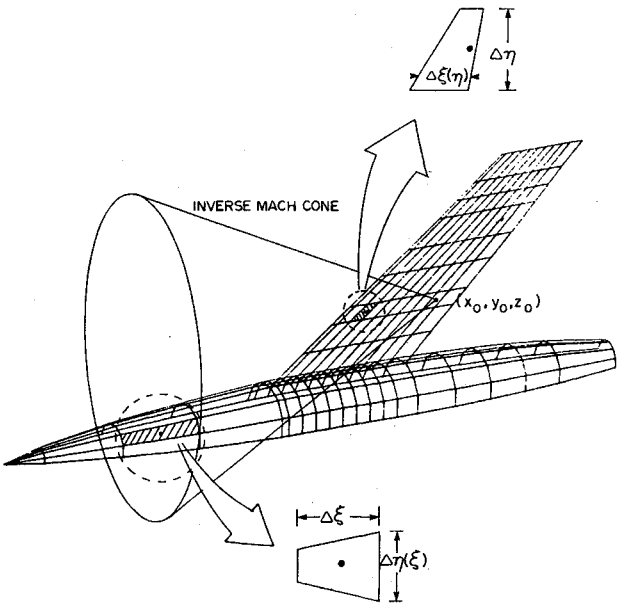

Fig. 1 Wing-body paneling scheme.

$$\phi_{z_{Bj}}=\frac{\partial\phi_{Bj}}{\partial z_0}=\int_{\Delta\xi}e^{-ikM\xi}\frac{\partial}{\partial z_0}(\psi)\,d\xi \tag{7}$$

Notice that Eqs. (5–7) contain steady VIC

$$\phi_{0x}=\int_{\Delta\xi}\frac{\xi\eta}{Rr^2}\,d\xi$$

$$\phi_{0y}=\int_{\Delta\xi}\frac{1}{R}\,d\xi$$

$$\phi_{0z}=\int_{\Delta\xi}\frac{\zeta\eta}{Rr^2}\,d\xi$$

which involve singular integrands of order $1/R$. However, these VICs are integrable singularities and, in fact, they can be integrated analytically and expressed in terms of elementary transcendental functions (see Ref. 16).

Through integration by parts, Eqs. (5–7) can be reduced to the regular integrals, which can then be integrated by the standard numerical schemes.

Boundary Conditions

For an arbitrary elastic body performing oscillatory motion with general flexible modes, its boundary condition in a body-fixed coordinate system has been derived by Garcia-Fogeda and Liu.[10] In a general form, it can be expressed as

$$V_B\cdot n=F_B(n,\,u,\,h_B^{(n)};\,K,\,M,\,\tau) \tag{8}$$

on the body surface, $r=R(x,\theta)$.

On the other hand, the boundary condition for the oscillating lifting surfaces is the well-known expression

$$V_w\cdot n=F_w(h_w,\,h_w';\,K) \tag{9}$$

on the mean wing surface, where $F_w=h_w'+iKh_w$.

In passing, it should be noted that the body boundary condition [Eq. (8)] involves the influence of steady mean flow and, hence, the body thickness τ, whereas the wing boundary condition totally decouples from these factors. More important, in the slender body limit as τ approaches zero, the function F_B should not reduce to the function F_w of Eq. (9).

In the subsonic domain, the NLR group has attempted to solve the wing-tip tank-store problem.[15] It is believed that the

boundary conditions on the bodies are not properly defined, and the slender body limit in terms of the NLR panel scheme remains to be clarified.

Source and Doublet Strengths

Since the steady mean-flow velocity components enter through the body boundary condition [Eq. (8)], these must be solved first using a similar procedure to that of USSAERO.

Once the right-hand side of Eq. (8) is known, the unsteady source and doublet strengths for a given wing-body configuraton can be solved along the surface according to the following matrix equation, i.e.,

$$\begin{bmatrix} \left(\frac{\partial\phi}{\partial n}\right)_{BB} & \left(\frac{\partial\phi}{\partial n}\right)_{BW} \\ \left(\frac{\partial\phi}{\partial n}\right)_{WB} & \left(\frac{\partial\phi}{\partial n}\right)_{WW} \end{bmatrix} \begin{Bmatrix} \sigma \\ \lambda \end{Bmatrix} = \begin{Bmatrix} F_B \\ F_W \end{Bmatrix} \tag{10}$$

where

$\left(\frac{\partial\phi}{\partial n}\right)_{BB}$ = the normal velocity influence coefficient induced by the body onto itself

$\left(\frac{\partial\phi}{\partial n}\right)_{WB}$ = the body on the wing

$\left(\frac{\partial\phi}{\partial n}\right)_{BW}$ = the wing on the body

$\left(\frac{\partial\phi}{\partial n}\right)_{WW}$ = the wing onto itself

Thus, the unsteady potential ϕ and the velocities u, v, and w can be obtained by multiplying the source strength and doublet strength by the potential and velocity influence coefficient matrices, respectively.

Pressure Coefficient and Generalized Forces

Based on the work of Garcia-Fogeda and Liu,[10] the unsteady pressure coefficient expressed in the body-fixed coordinate reads

$$C_p = -2S_0 \cdot [L_0 + iKL_1]$$

where

$$S_0 = \left[1 - \frac{\gamma-1}{2} M^2(2u_0 + u_0^2 + v_0^2 + w_0^2)\right]^{\frac{1}{\gamma-1}} \tag{11a}$$

$$L_0 = L_0(u_0, v_0, w_0, u, v, w, h_B^{(n)}) \tag{11b}$$

$$L_1 = L_1(u_0, v_0, w_0, \phi, h_B^{(n)}) \tag{11c}$$

The generalized forces can be expressed in terms of the mode functions h_{Bi} and h_{wi} and the pressure coefficient C_p, i.e.,

$$Q_{IJ} = \sum_{i=1}^{NB} C_{pi}^{(J)} A_i (n_{xi} h_{Bi}'^{(I)} z_{0i} - h_{Bi}^{(I)} n_{zi}) + \sum_{i=1}^{NW} C_{pi}^{(J)} A_i h_{wi}^{(I)} \tag{12}$$

Results and Discussion

To validate the present program, a series of numerical studies were performed and the following results were verified with available theoretical and measured data. The present numerical study proceeds with computations of body-alone cases and these are followed by the wing-body cases.

Table 1 Figures for body and wing/body

	Body	Wing and body
Steady ($K=0$)	Fig. 2	Fig. 5
Low frequency	Fig. 3	Figs. 6–11
Full frequency	Fig. 4	Figs. 12–21

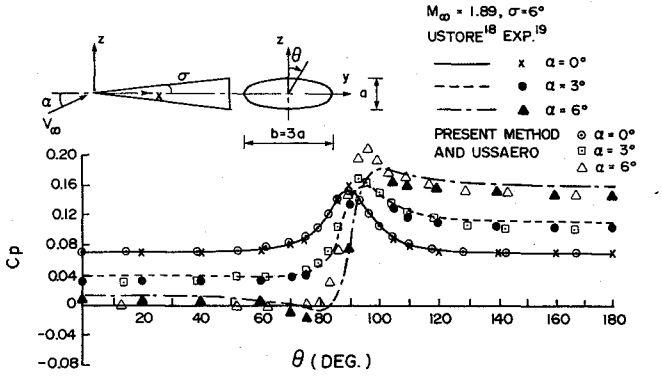

Fig. 2 Circumferential steady pressure distributions on an elliptic cone at various angles of attack.

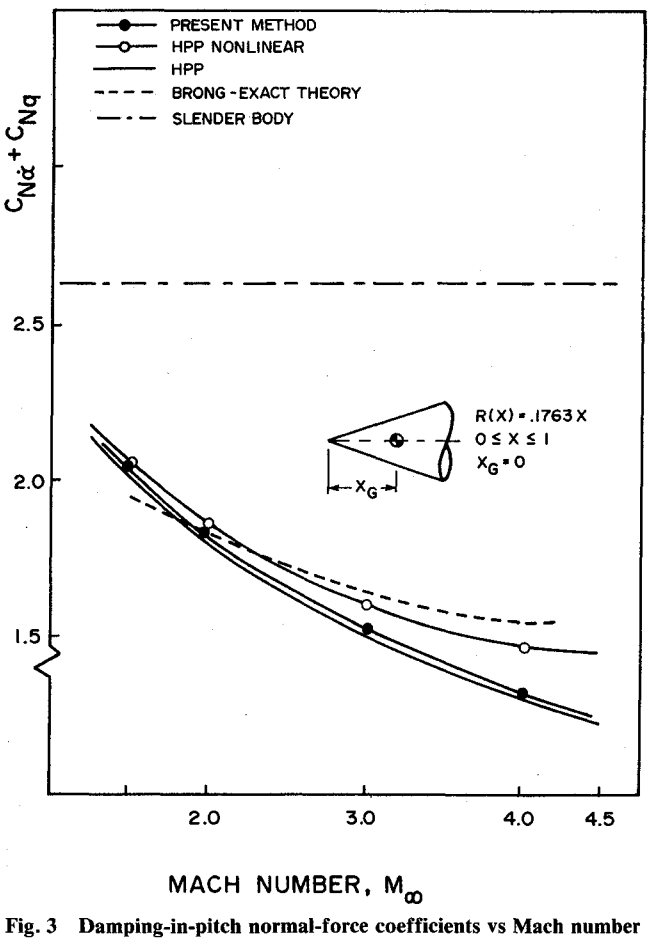

Fig. 3 Damping-in-pitch normal-force coefficients vs Mach number for a right circular cone.

Because of numerous cases involved in this study, Table 1 is provided to indicate the discussion sequence.

Elliptic Cone

Figure 2 presents pressure distribution on an elliptic cone ($\sigma = 6$ deg) at steady mean angles of attack, $\alpha_0 = 0$, 3, and 6 deg. The present computed results are compared with those of

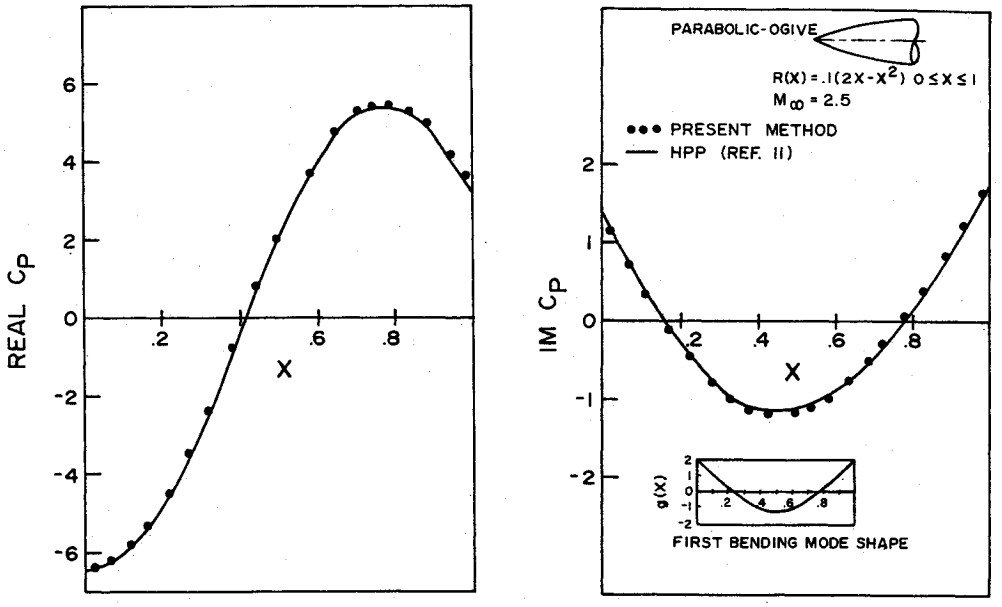

Fig. 4 In-phase and out-of-phase pressure coefficients for a bolic-ogive in first bending mode at $M_\infty = 2.5$ and reduced frequency $k = 1.0$.

the USTORE code[18] the USSAERO code,[16] and the measured data.[19] It should be noted that the present method practically recovers the results of the USSAERO code. This is expected since the present method is based on the generalized surface-panel schemes that contain the USSAERO formulation as a special case for $K = 0$. A parallel checking on the same case has been conducted using the line-doublet panel method (HPP method, Ref. 20). Our preliminary results indicate that the present surface-panel scheme is superior to the HPP method when the ellipticity ratio a/b (where a and b represent the major and minor axes of the ellipse) is below 1/3.

Oscillating Cone

For low-frequency cases, our computed results are verified with those computed and measured in terms of the damping stability derivatives for a right circular cone in oscillation. Figure 3 compares normal damping force coefficient for a 10-deg circular cone pitching about its apex as computed by various methods.[21] The present result is in excellent agreement with the HPP linear results,[11] as expected.

Ogive in First Bending

In Fig. 4, in-phase and out-of-phase pressures for a 10%-thick ogive body performing oscillation in a first bending mode are presented. Complete agreement is found between the HPP results and the present results in this high reduced-frequency case ($K = 1.0$). It should be noted that for the cases of oscillating cone and ogive, the numerical verifications are conducted in Figs. 3 and 4 with an aim to validate the present surface-panel method as opposed to the line-singularity method (HPP method) previously developed.[11] As such, the verification procedure is critical in that the accuracy of the present method for bodies and, hence, its expendability to a viable wing-body method, can be properly evaluated.

Steady Wing-Body Interface

Longitudinal loadings ($C_n d/d_{\max}$) over a 10% thick body with and without a tapered wing ($\mathcal{R} = 4.0$ and taper ratio $= 0.6$) are presented in Fig. 5

The force coefficient C_n is defined as

$$C_n = \frac{1}{d}\int_0^{2\pi} C_p \, d\theta \tag{13}$$

where d and $d_{\max}$ represent the diameter and maximum diameter of the body, respectively.

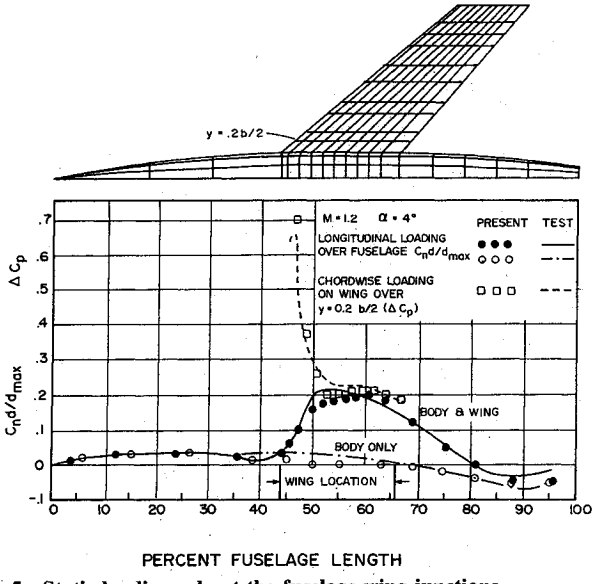

Fig. 5 Static loadings about the fuselage-wing junctions.

No interference effect is noted in the first 40% of the body length, as expected. A bump-like loading along 40–85% body length is observed as a result of the presence of the tapered wing. In addition, lifting pressure distribution along the wing chord is also plotted at the 20% semispanwise location. Good agreement is found between the computed and measured results.[22] Thus, the steady aerodynamic option of the present method is validated by means of this present interference example.

NACA Wing-Body Configuration

To verify our computed results for wing-body combinations in the low-frequency limit, measured stability derivatives for a delta wing body with $\mathcal{R} = 2$ (Fig. 6) in NACA RM A52104a were selected for comparison.[23]

The stability derivatives in this case are expressed in terms of the generalized forces Q_{IJ}, i.e.,

$$C_{L_\alpha} = \frac{Re(Q_{12})}{S} \tag{14a}$$

$$C_{M_\alpha} = \frac{Re(Q_{22})}{S\bar{c}} \tag{14b}$$

$$C_{M_q} + C_{M_{\dot{\alpha}}} = 2\frac{I_m(Q_{22})}{S\bar{c}K} \tag{14c}$$

where S is the wing area, $\bar{c}$ the mean aerodynamic chord, K the reduced frequency based on $\bar{c}$, $K = \omega\bar{c}/U_\infty$ (where ω is the circular frequency), and Q_{12}, Q_{22} are the 12 and 22 components of the computed 2×2 generalized forces matrix with two rigid-body modes. The first one is the plunging mode and the second one is the pitching mode.

Figure 7 presents the computed lift curve slopes C_{L_α} for the body only, wing only, and the wing-body cases. It is seen that the wing-only case (a delta wing as shown in Fig. 6) produces the highest lift slope as expected, whereas, by constrast, the body-only case produces a relatively insignificant lift slope throughout the Mach number ranges. Notice that the present C_{L_α} value is based on the wing surface area. Typical C_{L_α} for bodies uses the base area. A conversion formula reads:

$$(C_{L_\alpha})_{\text{present}} = \left(\frac{\text{wing area}}{\text{body base area}}\right)(C_{L_\alpha})_{\text{body}} \tag{15}$$

The present wing-body result tends to underpredict C_{L_α} slightly, whereas in Figs. 8 and 9 the pitching moments C_{M_α} (about pitching axis $0.35\bar{c}$ and $0.45\bar{c}$) for wing and body appear to be in better agreement with the test data then the wing-only results.

However, the damping-in-pitch moments at these locations, as shown in Figs. 10 and 11, indicate slight overprediction of the present wing-body results, whereas the wing-only results are in better agreement with the measured data.

It should be noted that the slight overprediction of the stiffness and damping moments by the present method in comparison with the measured data could be subject to a number of factors. These include the aeroelastic effect of the wind-tunnel model as well as the induced viscous effects as pointed out previously in Ref. 23.

NLR Underwing Store

In Fig. 12, a NLR wind-tunnel test configuration constructed with an F-5 wing plus an underwing store is modeled by 112 body panels representing the missile body, 72 wing panels for the launcher, and 24 panels for the four aft fins.

The complete configuration is in pitching oscillation about 50% root chord at a circular frequency $F = 20$ Hz, and at two Mach numbers, $M = 1.1$ and 1.35.

In Figs. 13–15, the comparisons of the NLR measured data[17] and the present computed results are presented. The unsteady force and moment coefficients used in these figures are defined as follows:

The store normal-force coefficient is

$$C_{Z_i} = \frac{Z_i}{\pi\bar{c}S} \tag{16}$$

where Z_i is the computed normal force.

The side-force coefficient is

$$C_{Y_i} = \frac{Y_i}{\pi\bar{c}S} \tag{17}$$

where Y_i is the computed side force.

The pitching-moment coefficient is

$$C_{M_i} = \frac{M_i}{\left(\frac{\pi}{2}\right)\bar{c}^2 S} \tag{18}$$

where M_i is the computed pitching moment.

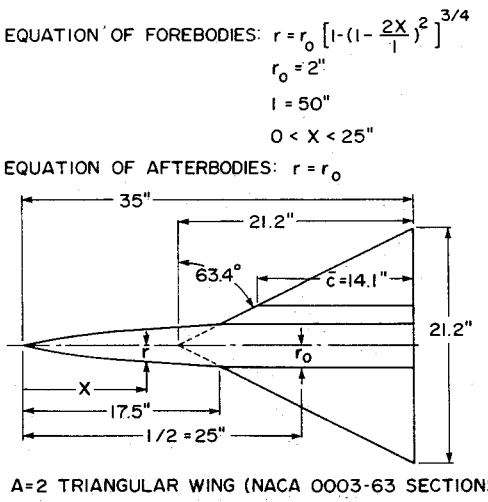

Fig. 6 Sketch of a wing-body combination: $\mathcal{R} = 2.0$ delta wing with centered body of revolution.

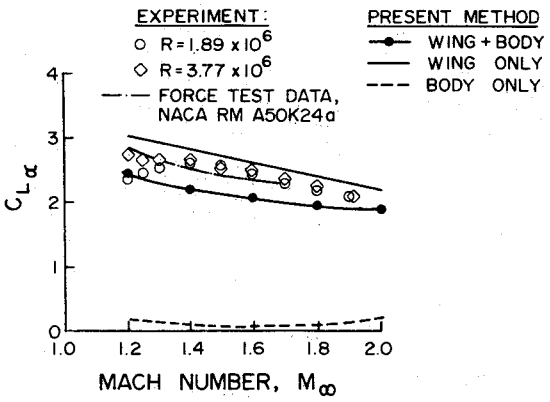

Fig. 7 Lift-curve slopes for an $\mathcal{R} = 2.0$ wing-body combination.

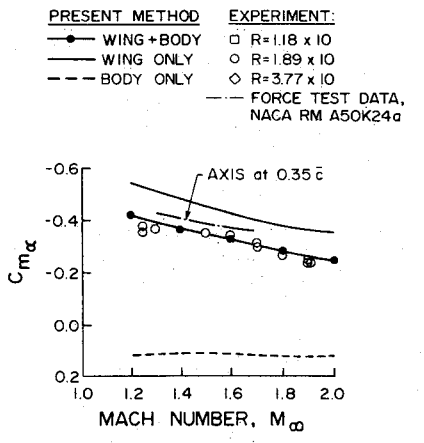

Fig. 8 Moment-curve slopes for an $\mathcal{R} = 2.0$ wing-body combination about pitching axis at $0.35\bar{c}$.

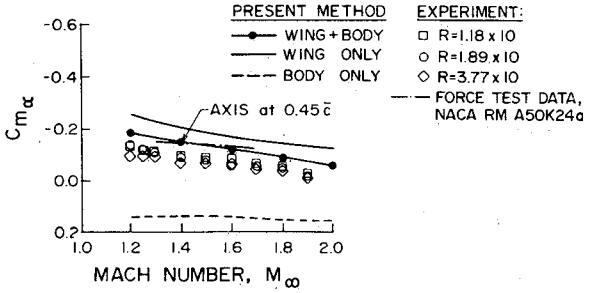

Fig. 9 Moment-curve slopes for an $\mathcal{R} = 2.0$ wing-body combination about pitching axis at $0.45\bar{c}$.

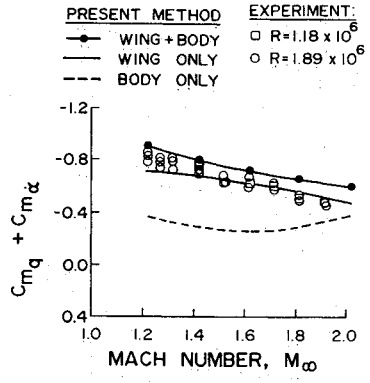

Fig. 10 Damping-in-pitch moment coefficients for an $\mathcal{R}=2.0$ wing-body combination about pitching axis at 0.35c.

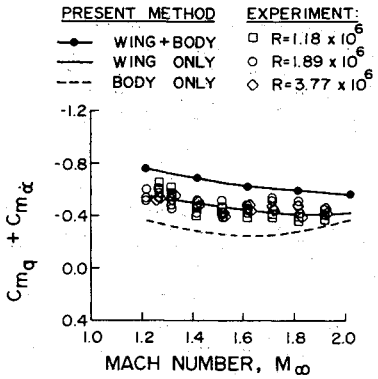

Fig. 11 Damping-in-pitch moment coefficients for an $\mathcal{R}=2.0$ wing-body combination about pitching axis at 0.45c.

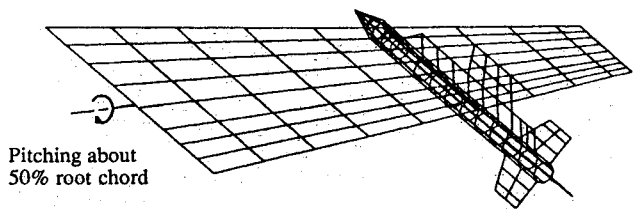

Fig. 12 Paneling model for the underwing store configuration: Northrop F-5 wing plus underwing pylon, launcher, missile body with four aft fins.

The yawing-moment coefficient is

$$C_{N_i}=\frac{N_i}{\left(\frac{\pi}{2}\right)\bar{c}^2 S} \tag{19}$$

where N_i is the computed yawing moment, $\bar{c}=0.4183$ the mean geometric chord, and $S=0.6226$ the semispan.

Figure 13 presents the unsteady normal forces and pitching moments on the underwing store system of two different combinations: 1) the pylon plus launcher ($P+L$), and 2) in addition to 1), a missile body with four aft fins ($P+L+MB+AW$). The in-phase (real) part of the computed normal forces and pitching moments for both cases correlated well with the measured data, while all out-of-phase (imaginary) parts remain insignificantly small.

Figure 14 presents the side forces and yawing moments on the underwing store systems in three different combinations: 1) pylon alone (P); 2) pylon and launcher ($P+L$); and 3) in addition to 2), a missile body with four aft fins ($P+L+MB+AW$). Both measured data and computed results show increases in the in-phase normal forces (positive for outboard direction) with the addition of the system from 1) to

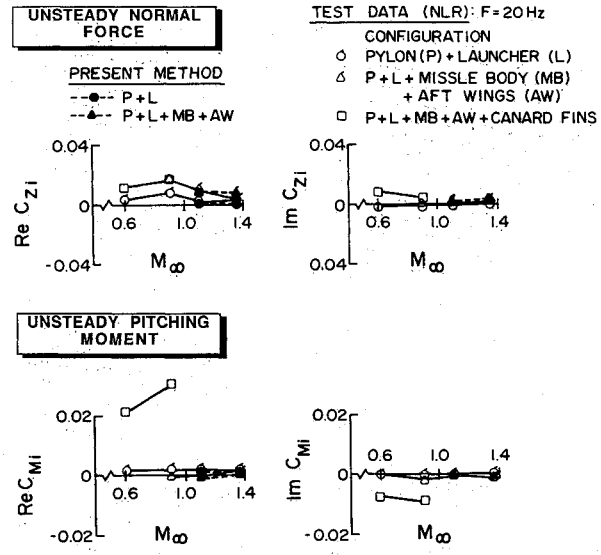

Fig. 13 Unsteady normal force and pitching moment for the underwing store configuration with and without the missile body oscillating about 50% root chord at $M_\infty=1.1$ and 1.35 and reduced frequency $k=0.1$.

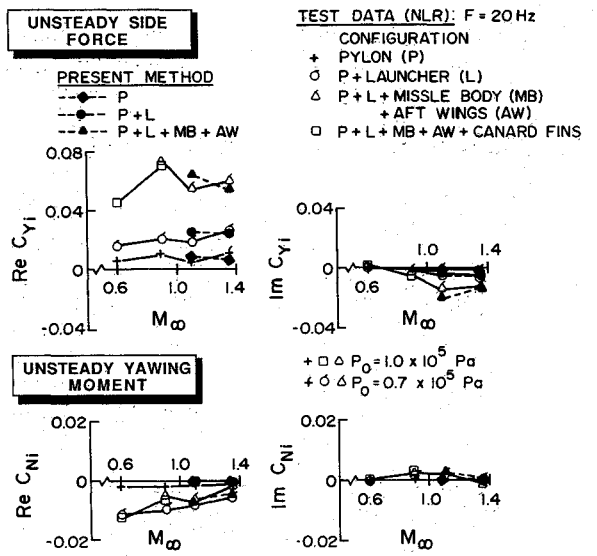

Fig. 14 Unsteady side force and yawing moment for the complete underwing store configuration with and without the missile body and launcher oscillating about 50% root chord at $M_\infty=1.1$ and 1.35 and reduced frequency $k=0.1$.

3), whereas a decreasing trend is observed for the out-of-phase parts. The unsteady yawing moments on the system are relatively small. The computed results also show that the added missile with fins to the system contributes most to the in-phase moment (positive body apex pointing inboard). In Fig. 15, the integrated spanwise unsteady normal forces and pitching moments along the F-5 wing under the influence of the complete underwing store system are plotted against those of the clean-wing case according to the computed results and the test data.

The unsteady force and moment coefficients in this figure are defined as follows:

The section normal force is

$$C_{zi}=\frac{1}{\pi}\int_0^1 \Delta C_p \,\mathrm{d}(x/c) \tag{20}$$

The section pitching moment is

$$C_{mi}=\frac{2}{\pi}\int_0^1 \Delta C_p (x/c-0.25)\,\mathrm{d}(x/c) \tag{21}$$

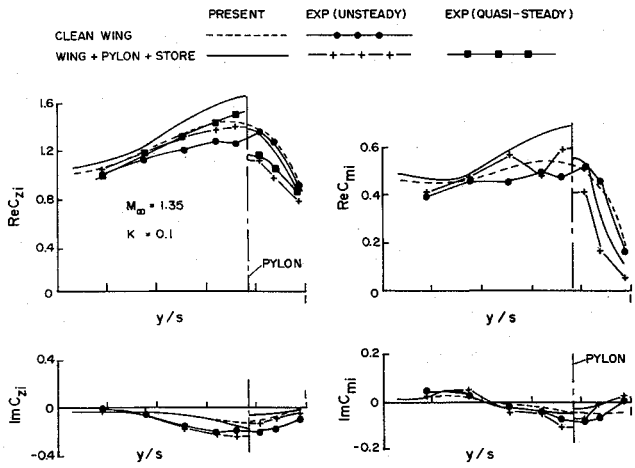

Fig. 15 Unsteady spanwise normal force and pitching moment for the clean F-5 wing and the underwing store configuration at $M_\infty = 1.35$ and reduced frequency $k = 0.1$.

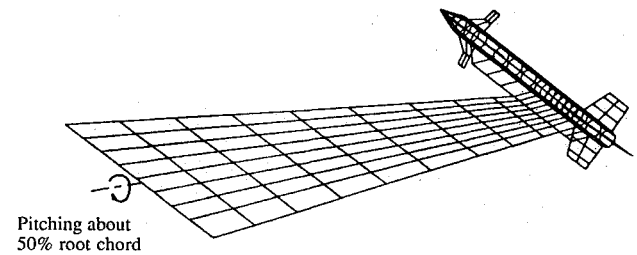

Fig. 16 Paneling model for the wing-with-tip missile configuration: Northrop F-5 wing plus launcher, missile body with fore and aft fins.

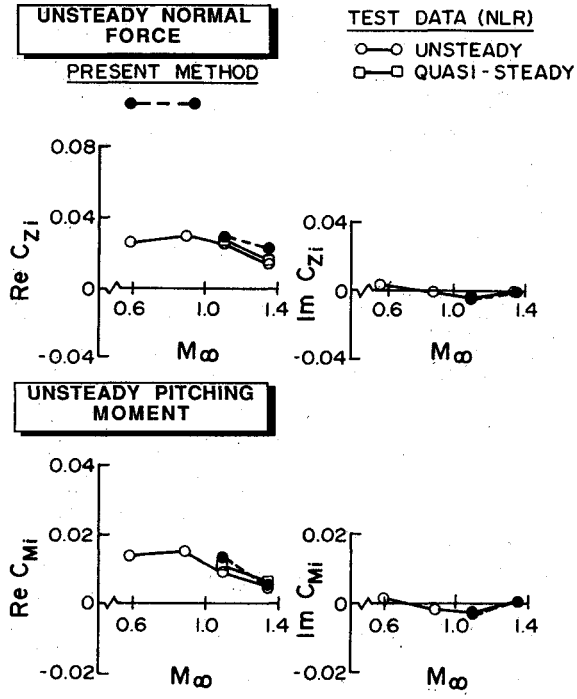

Fig. 17 Unsteady normal forces and pitching moments for the F-5 wing plus tip launcher oscillating about 50% root chord at $M_\infty = 1.1$ and 1.35 and reduced frequency $k = 0.1$.

where c is the local chord length.

It is seen that the computed forces and moments predict the same trend as the measured data showing a finite discontinuity across the pylon location. The computed results tend to overestimate the in-phase forces and moments and underestimate

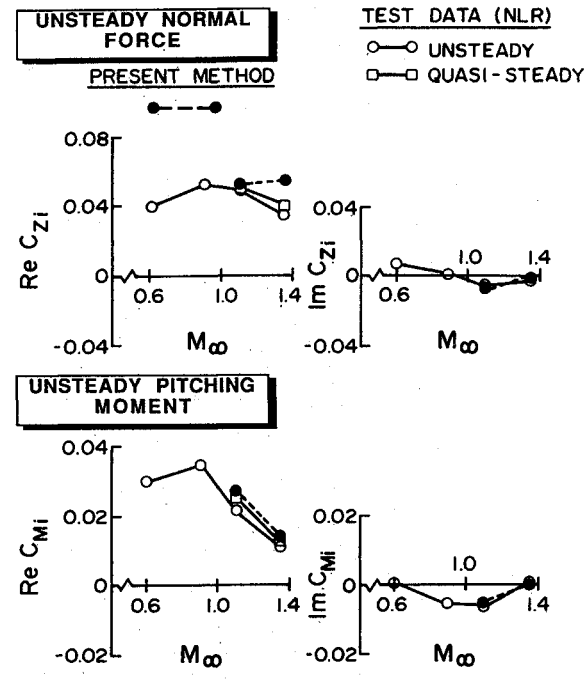

Fig. 18 Unsteady normal forces and pitching moments for the F-5 wing plus tip launcher and tip missiles at $M_\infty = 1.1$ and 1.35 and reduced frequency $k = 0.1$.

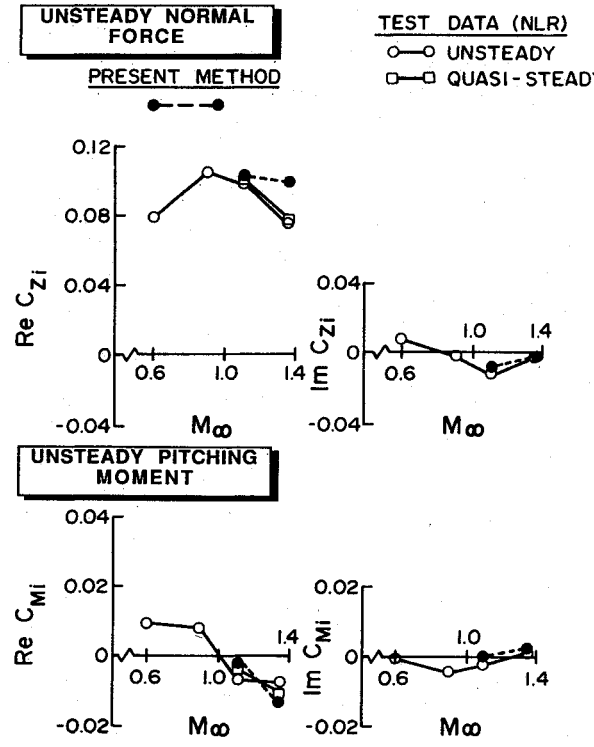

Fig. 19 Unsteady normal forces and pitching moments for the F-5 wig plus tip launcher and missile body with aft fins at $M_\infty = 1.1$ and 1.35 and reduced frequency $k = 0.1$.

the out-of-phase forces and moments in comparison with the measured data.

However, these discrepancies may be caused by the uncertainties in the measured unsteady data as mentioned in Ref. 17. Meanwhile, NLR also provided the measured quasisteady data, which is supposedly more reliable for the in-phase forces. Better agreement in trend between the quasisteady data and the computed results is found for this case.

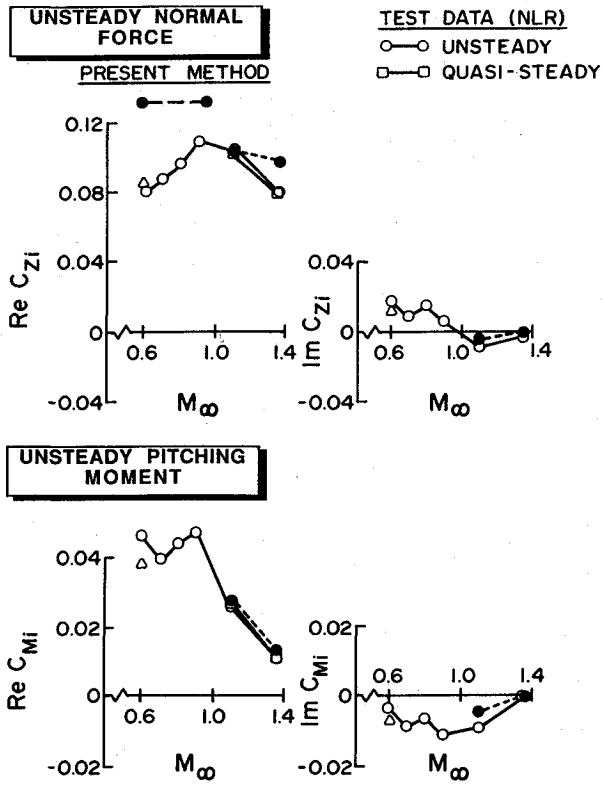

Fig. 20 Unsteady normal forces and pitching moments for the complete wing-with-tip missile configuration at $M_\infty = 1.1$ and 1.35 and reduced frequency $k = 0.1$.

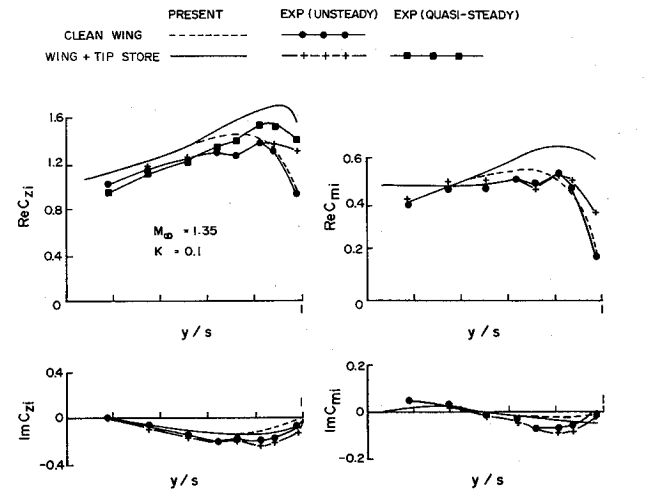

Fig. 21 Unsteady spanwise normal force and pitching moment for the clean F-5 wing and the complete wing-with-tip missile configuration at $M_\infty = 1.35$ and reduced freqency $k = 0.1$.

NLR Wing-with-Tip Missile

In Fig. 16, another NLR wind-tunnel test configuration constructed with an F-5 wing-with-tip missile is modeled with 72 wing panels for the F-5 wing, 14 panels for the pylon, 16 panels for the four canard fins, 24 panels for the four aft fins, and 112 body panels for the missile body. This configuration was tested under the same conditions as those provided for the NLR underwing store cases.

The normal forces and pitching moment computed for the present configuration consists of four cases: 1) the tip launcher only (Fig. 17); 2) the tip launcher plus missile body (Fig. 18); 3) the tip launcher plus missile body with four aft fins (Fig. 19); and 4) the complete tip missiles, all in 3) plus four canard fins (Fig. 20). For all cases considered, the computed results are generally in good agreement with the NLR measured data with the exception of normal-force predictions at $M_\infty = 1.35$.

It is interesting to see that the aft fins produce a stabilizing moment in Fig. 20, whereas they completely negate the moment contribution due to the missile body and the launcher in Figs. 17 and 18.

By comparing Fig. 20 to Fig. 19, it is seen that the pitching moment is changed from a stable region to an unstable one due to the addition of four canard fins, whereas the changes in normal forces are small. The present results not only follow the overall trends in measurement but also provide accurate prediction in almost every case.

Lastly, the unsteady spanwise normal forces and pitching moments for a clean F-5 wing and the complete wing-with-tip missile are plotted along the semispan in Fig. 21.

Departure between the results obtained for the clean wing and the wing-with-tip missile cases starting from 60% semispan toward the wing tip are observed. This is expected since the influence domain of the tip missile to the wing is bounded by the forward Mach cone emanating from the missile apex.

Similar to Fig. 15, the computed results in the present case tend to overpredict the out-of-phase forces and moments in comparison with the measured data. Again, these discrepancies may be caused by the uncertainties in the measurement, as mentioned in Ref. 17. Better agreement in trends between the more reliable NLR quasisteady data and the present results can be seen for this case.

In particular, the discrepancies between the present results and those measured, shown in the lift curve slopes for the NACA wing-body (Fig. 7) and in the forces and moments for the wing-with-tip missile (Figs. 18 and 19), appear to have 5–20% error. Other than the causes suggested above, further studies in the paneling refinements are warranted in order to verify with the measured data.

Conclusions

A general method has been developed to compute the unsteady aerodynamics for arbitrary wing-body configuration including external stores in supersonic flow. The present method generalizes the harmonic gradient method for wings to include treatments for arbitrary wing-body combinations.

The harmonic gradient model used assures that the panel number required is least affected by the given Mach number and reduced frequencies. To verify with available theory and measured data, numerous cases are computed for body, wing-body and wing-with-external stores configurations.

Good agreement is found for all cases considered. Accurate prediction by the present method also quantitatively confirms the trends in NLR measured forces and moments for a Northrop F-5 wing with under wing store and wing-with-tip-missile configurations.

Meanwhile, a computer program has been developed for aeroelastic applications to realistic aircraft configurations. This program contains salient features such as 1) it has built-in subsystems for ease of input, 2) valid for all reduced frequencies, and 3) for complex wing-body combinations with any given modes, etc. Therefore, it is believed that a well-developed method and a production-ready three-dimensional unsteady supersonic code for arbitrary wing-body combinations are finally at hand.

References

[1]Rodden, W. P., Giesing, J. P., and Kalman, T. P., "New Developments and Applications of the Subsonic Doublet-Lattice Method for Nonplanar Configurations," AGARD Symposium on Unsteady Aerodynamics for Aeroelastic Analyses of Interfering Surfaces, Paper No. 4, May 1970.

[2]Giesing, J. P. and Kalman, T. P., "Oscillatory Supersonic Lifting Surface Theory Using a Finite-Element Doublet Representation," AIAA Paper 75-761, 1975.

[3]Cunningham, A. M., Jr., "Oscillatory Supersonic Kernel Function Method for Interfering Surface," *Journal of Aircraft*, Vol. 11, No. 11, 1974, pp. 664–670.

[4]Cunningham, A. M., Jr., "Oscillatory Supersonic Kernel Function Method for Isolated Wings," *Journal of Aircraft*, Vol. 11, No. 10, 1974, pp. 609–615.

[5]Jones, W. P. and Appa, K., "Unsteady Supersonic Aerodynamic Theory for Interfering Surface by the Method of Potential Gradient," NASA CR-2898, Oct. 1977.

[6]Hounjet, M. H. L., "An Improved Potential Gradient Method to Calculate Airloads on Oscillating Supersonic Interfering Surfaces," *Journal of Aircraft*, Vol. 19, No. 5, 1982, pp. 390–399.

[7]Ueda, T. and Dowell, E. H., "Doublet-Point Method for Supersonic Unsteady Lifting Surfaces," *AIAA Journal*, Vol. 22, Feb. 1984, pp. 179–186.

[8]Lottati, I. and Nissim, E., "Nonplanar Supersonic Three-Dimensional Oscillatory Piecewise Continuous Kernel-Function Method," *Journal of Aircraft*, Vol. 24, Jan. 1987, pp. 45–54.

[9]Chen, C. P. and Liu, D. D., "A Harmonic Gradient Method for Unsteady Supersonic Flow Calculations," *Journal of Aircraft*, Vol. 22, May 1985, pp. 371–379.

[10]Garcia-Fogeda, P. and Liu, D.D., "A Harmonic Potential Panel Method for Flexible Bodies in Unsteady Supersonic Flow," AIAA Paper 86-007, 1986; also, *Journal of Aircraft*, Vol. 24, Dec. 1987, p. 833–840.

[11]Garcia-Fogeda, P. and Liu, D. D., "Aeroelastic Applications of Harmonic Potential Panel Method to Oscillating Flexible Bodies in Supersonic Flow," *Journal of Spacecraft and Rockets*, Vol. 25, July–Aug. 1988, pp. 271–277.

[12]Liu, D. D., Garcia-Fogeda, P. and Chen, P. C., "Oscillating Wings and Bodies and Flexure in Supersonic Flow—Applications of Harmonic Potential Panel Method," *Journal of Aircraft*, Vol. 25, June 1988, pp. 507–514.

[13]Morino, L., Chen, L. T., and Suciu, E. O., "Steady and Oscillating Subsonic and Supersonic Aerodynamics Around Complex Configuration," *AIAA Journal*, Vol. 13, March 1975, pp. 368–374.

[14]Sotomayer, W. A., Dusto, A. R., Epton, M. A., and Johnson, F. T., "Aerodynamic Modeling of Oscillating Wing With External Stores," AIAA Paper 81-0648, May 1981.

[15]Roos, R., Bennekers, B., and Zwann, R. J., "A Calculation Method for Unsteady Subsonic Flow About Harmonically Oscillating Wing-Body Configuration," AIAA Paper 75-854, 1975.

[16]Woodward, F. A., "An Improved Method for the Aerodynamic Analysis of Wing-Body-Tail Configurations in Subsonic and Supersonic Flow," NASA CR-2228, May 1973.

[17]Tijdeman, J. et al., "Transonic Wind-Tunnel Tests on an Oscillating Wing with External Stores; Part I-IV, the Wing with Tip Store," Air Force Flight Dynamics Laboratory, Wright Patterson AFB, OH, AFFDL-TR-78-194, May 1979.

[18]Van der Broek, G. J., "The Analytical Prediction of the Separation Behavior of External Stores after Release From the Carrier Aircraft, Part II—Applications," NIAST 79/103, Aug. 1979.

[19]Maslen, S. H., "Pressure Distribution on Thin Conical Body of Elliptic Cross Section at Mach Number 1.89," NACA RM E8K05, 1949.

[20]Garcia-Fogeda, P. and Liu, D. D., "Three-Dimensional Analysis of Supersonic Flows Around Arbitrary Bodies Using Boundary Collocation Method," *Boundary Element Techniques: Applications in Fluid Flow and Computational Aspects*, edited by C.A. Brebbia and W.S. Venturini, Computational Mechanics Publications, 1987, pp. 75–88.

[21]Platzer, M. D. and Sherer, A. D., "Dynamic Stability Analysis of Bodies of Revolutions in Supersonic Flow," *Journal of Spacecraft and Rockets*, Vol. 5, July 1968, pp. 833–837.

[22]Loving, D. L. and Estabrooks, B. B., "Transonic-Wing Investigation in the Langley 8-Foot High-Speed Tunnel at High Subsonic Mach Numbers and a Mach Number of 1.2," NACA RM L51F07, Sept. 1951.

[23]Tobak, M., "Damping-in-Pitch of Low-Aspect-Ratio Wings at Subsonic and Supersonic Speeds," NACA RM A52L04a, 1953.